WCCM V
Fifth World Congress on
Computational Mechanics
July 7–12, 2002, Vienna, Austria
Eds.: H.A. Mang, F.G. Rammerstorfer,
J. Eberhardsteiner

Numerical Investigation of the Entrainment of Flux into the Lubrication Gap in Continuous Casting of Steel

Herbert Steinrück*, Christian Rudischer

Institute of Fluid Dynamics and Heat Transfer
Christian Doppler Laboratory for Continuous Solidification Processes
Vienna University of Technology, Resselgasse 3, A–1040 Vienna, Austria
e-mail: herbert.steinrueck@tuwien.ac.at

Key words: Coating, Solidification, Continuous Casting, Oscillation Marks

Abstract
A model for the formation of oscillation marks in continuous casting of steel will be derived and evaluated numerically.
Liquid steel is injected through a submerged nozzle into an intensively cooled mould. At the wall the steel solidifies and the solidified shell is withdrawn vertically. Flux powder is added at the top of liquid steel. It melts (slag) and thus it serves as a lubricant for the passage of the steel shell through the mould. In order to prevent sticking of the steel onto the mould it oscillates vertically leaving oscillation marks on the surface of the solidified steel shell.
In the present study the interaction of the steel melt, the solidified steel shell and the slag will be investigated. On the basis of thin layer approximations for the slag flow and heat transfer through the steel shell, slag and mould, respectively, and dominating surface tension at the interface liquid steel/liquid slag a mathematical model will be derived, solved numerically and compared with data reported in the literature. The flow problem for the slag flow is closely related to the well known coating problem.

1 Introduction

Continuous casting is a method of producing an infinite solid strand from liquid metal by continuously solidifying it as it moves through a casting machine (fig. 1). Linking steel making and hot rolling, it has become the predominant process route in modern steel production.

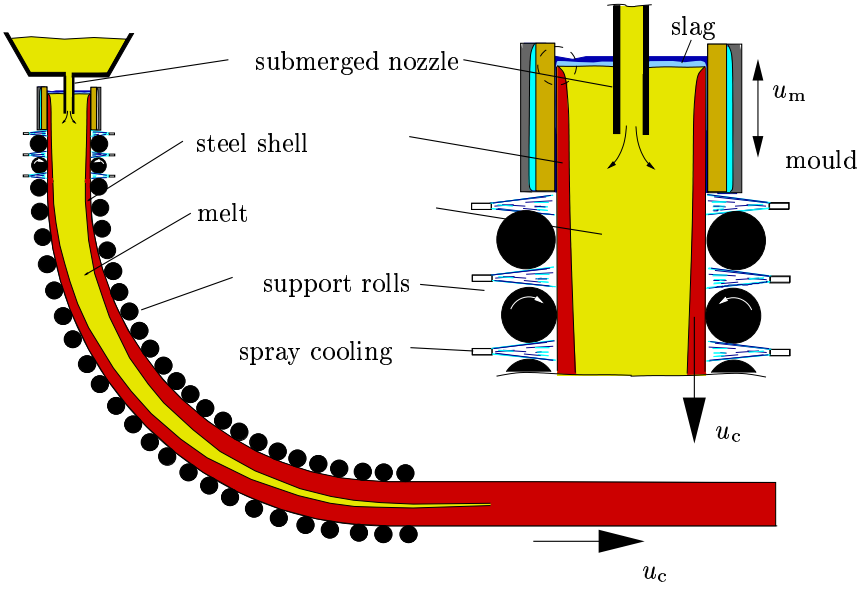

Figure 1: Continuous casting machine

Liquid metal is continuously fed into a copper mould through a submerged nozzle (fig. 1). Intense water cooling causes the metal to solidify, and by the time the metal strand leaves the mould vertically, a solid shell thick enough to withstand the ferro-static pressure of the liquid core must have formed. Outside the mould the shell is supported by support rollers. It is bent via an arc with a radius of about 10m into horizontal direction. Cooling is accomplished by water sprays and final solidification is achieved at the end of the arc.

The initial stages of solidification are crucial for the stability of the process and the quality of the strand surface. One measure to achieve that goals is to add casting powder *(flux, slag)* (fig. 2) at the top of the mould. It melts and fills a thin gap between the mould and the metal strand. This serves to lubricate the passage of the metal through the mould and to prevent direct thermal contact between the two, which would cause the strand to freeze onto the mould and consequently lead to shell rupture and liquid metal being spilt below the mould. Reciprocation of the mould has turned out to improve the reliability of the continuous casting process, but it also causes unwanted dents in the strand surface *(oscillation marks)*. The mechanisms of these two effects are still not completely understood.

Metallurgical examinations have shown that there are at least two fundamentally different ways in which oscillation marks can form [8]: A pressure difference between the molten flux and the melt can bend the solidified meniscus cusp, leaving a depression in the strand shell. Alternatively, the solidified meniscus can be overflowed by liquid metal and remain as a thumb nail trace microstructure. Both types of oscillation marks are distinguished from *ripple marks*, which are not directly related to the mould oscillation and can also occur with a static mould.

The *meniscus bending*-type oscillation marks are strongly affected by the fluid flow in the flux gap. Therefore, both analytical and numerical calculations have been performed for quite some time to deter-

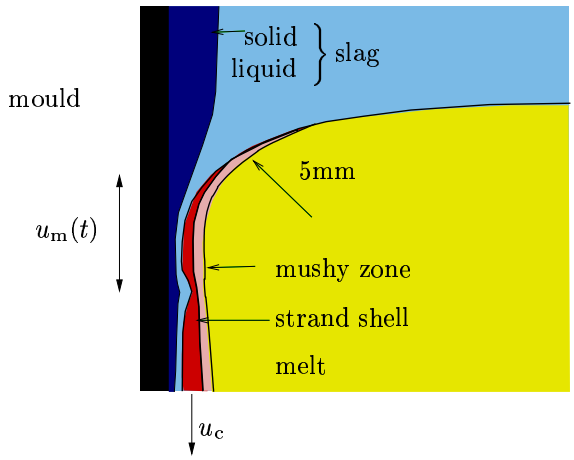

Figure 2: The meniscus region

mine how changes in the flux properties or in the mould oscillation mode can improve the surface quality of the cast strand.

The first of these simulations [4, 22, 1, 3, 18] used a fixed shape of the flux gap to calculate the fluid flow and/or heat transfer. Others [15, 7, 10] account for the interdependence of the shape of the flux gap and the fluid flow therein, but still require some parameter — either the gap width or the pressure at a given point — to be prescribed rather arbitrarily, unless it can be taken from measurements.

A recent investigation [19] overcomes this handicap by assuming that the gap width is determined by the interfacial tension between liquid metal and liquid slag. However, the mechanical part of this simulation (fluid flow and deformation of the strand shell) is de-coupled from the thermal part (solidification of the shell). The thickness of the strand shell is computed from the time-averaged heat flux density at the mould (which is gained empirically) and remains unaffected by the mould oscillation.

In this study [20] a fully coupled, self-contained mathematical model for the formation of oscillation marks in continuously cast steel due to the *meniscus bending* mechanism will be presented. It comprises the interaction of fluid flow, heat transfer and solidification and requires only the knowledge of material properties and process parameters.

Starting from a two-dimensional view of the top part of the mould (the region near the meniscus), the theory of thin layers is applied. This approach is reasonable for the mould wall, the flux gap and the strand shell, not however for the turbulent flow of the melt (for which already the two-dimensional view would be an inappropriate simplification). Therefore, the melt flow is not covered by this model, and the heat transfer in the melt must be determined separately. This can either be done experimentally (e.g., by temperature measurements in the mould wall) [14, 5, 16, 24] or numerically (by some computational method suitable for three-dimensional turbulent flow) [9, 25, 12]. A second aspect not covered by the model presented here are differences between the broad faces, the narrow faces and the corner regions of the mould. Where those differences matter, this model best describes the center of a broad face.

A major advantage of the model is that slag flow, heat transfer and solidification of the strand shell are solved simultaneously. Changes in the shell thickness and the position of the shell tip during each oscillation cycle turn out to have substantial influence of the formation of oscillation marks. This influence has been neglected in previous works.

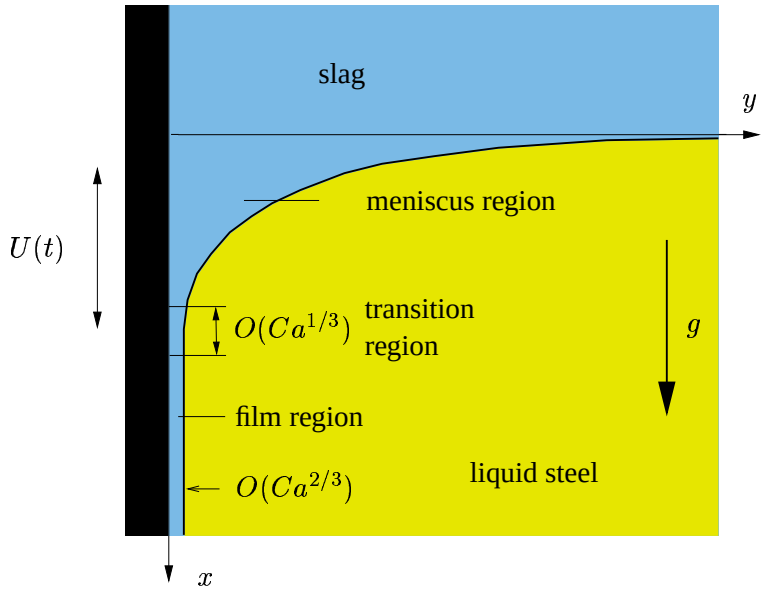

Figure 3: Three distinct regions of flow in the limit $Ca \to 0$.

2 Slag flow

To understand the fluid flow in the slag gap, a simplified problem without solidification can be studied. This problem is closely related to *free coating*, which is applied in many industrial processes such as the production of photographic film and has been studied extensively. The theory of free coating needs to be extended to the case of an oscillating wall. Thus the Laplace Capillary length

$$L = \sqrt{\frac{\gamma}{g(\rho_{\mathrm{st}} - \rho)}}, \tag{1}$$

where γ, g and ρ_{st}, ρ are the interfacial tension between slag and steel, the gravity acceleration and the densities of steel and slag, respectively, serves as a reference length.

In this study we assume for sake of simplicity that all material properties of the liquid slag to be constant, although they depend strongly on temperature. The capillary numbers $Ca = \mu u_{\mathrm{m}}/\gamma$ based on the mould velocity u_{m}, the slag viscosity μ and the interfacial tension γ describes the influence of the interfacial tension compared to the viscosity effects. An asymptotic analysis for small capillary numbers identifies three distinct regions (fig. 3): In the *meniscus region* the pressure in the slag is dominated by the hydrostatic part. The shape of the meniscus is therefore de-coupled from the fluid flow. In the *flux gap* the pressure is essentially equal to the ferro-static pressure of the adjacent melt. The velocity of the slag is constant across the gap *(plug flow)*, and the shape of the flux gap can be described by a kinematic wave equation. Note that there is no solid strand shell in this simplified problem. Finally, a short *intermediate zone* connects the meniscus region to the slag gap. It accomplishes the rapid rise of pressure from the hydrostatic value in the meniscus region to the higher level in the gap. In this intermediate zone the direction of the mould wall motion is crucial. In the case of the mould wall moving downwards, the problem is quasi-steady, and the gap width can be expressed by simply scaling a reference solution. Near the turning point of the mould, the problem is no longer quasi-steady, and a special scaling of coordinates — including time — is necessary. In the case of the mould wall moving upwards, the width of the flux gap is governed from the bottom part of the mould, which is not part of this model. However, any effects which might propagate upwards cannot — in a first-order approximation —- affect the meniscus region, nor do

they leave any trace to the next downstroke phase. All terms occurring in the asymptotic approximations are contained in a uniformly valid equation for the dimensionless gap width $\bar{w}$ which can be directly obtained using the lubrication approximation.

$$\bar{Q} = \bar{u}_{\mathrm{m}} \frac{1+\zeta_{\mathrm{s}}}{2}\bar{w} + \bar{u}_{\mathrm{sh}} \frac{1-\zeta_{\mathrm{s}}}{2}\bar{w} - \frac{(1-\zeta_{\mathrm{s}})^3 \bar{w}^3}{12Ca}\left(\frac{\partial \bar{p}}{\partial \bar{x}} + 1\right) . \tag{2}$$

The continuity equation over a cross section reads

$$\frac{\partial \bar{Q}}{\partial \bar{x}} + \frac{\partial \bar{w}}{\partial \bar{t}} = 0 . \tag{3}$$

Here $\bar{Q}$ denotes the dimensionless mass flow rate of flux, $\bar{p}$ the pressure in the flux gap, and $\bar{u}_{\mathrm{m}}$, $\bar{u}_{\mathrm{sh}}$ the velocity of the mould and strand shell, respectively. Due to the cooling of the mould the slag will freeze onto the mould wall. The width of the solidified slag layer is denoted by $\zeta_{\mathrm{s}}\bar{w}$.

In absence of a solidified strand shell the dimensionless pressure $\bar{p}$ is given by

$$\bar{p} = -\bar{\kappa} \tag{4}$$

where $\bar{\kappa}$ is the dimensionless curvature of the interface steel/slag.

The equations (1)-(3) are uniformly valid and therefore give a correct first-order approximation for the meniscus shape, even though the assumption of a thin layer is violated in the meniscus region.

3 Mechanical properties of the strand shell

The solid steel shell is treated as a thin plate under a transverse load due to the pressure difference between the flux gap and the mushy zone. A simple elasto-viscoplastic constitutive model is used, taking into account the variation of mechanical properties with temperature. Using a two term 'Galerkin' method we obtain an equation for the deformation of the plate:.

$$\frac{\partial \bar{\kappa}}{\partial \bar{t}} + \bar{U}_{\mathrm{cast}} \frac{\partial \bar{\kappa}}{\partial \bar{x}} = \frac{12}{\bar{E}\bar{d}_{\mathrm{s}}^3}\left(\frac{\partial \bar{M}}{\partial \bar{t}} + \bar{U}_{\mathrm{cast}} \frac{\partial \bar{M}}{\partial \bar{x}}\right) + \frac{6^{n+1}}{n+2}\frac{\bar{C}}{\bar{d}_{\mathrm{s}}^{2n+1}} \bar{M}|\bar{M}|^{n-1} . \tag{5}$$

The dimensionless material properties $\bar{E}$, n and $\bar{C}$ are taken at the interface temperature ϑ_{if}. The bending moment is denoted by $\bar{M}$ and the thickness of the solid shell by $\bar{d}_{\mathrm{s}}$. The strand shell moves with the casting speed $\bar{U}_{\mathrm{cast}}$ downward. The dimensionless pressure in the flux gap is given by,

$$\bar{p} = \frac{\partial^2 \bar{M}}{\partial \bar{x}^2}. \tag{6}$$

The mushy zone is split into two parts: The part with a solid fraction of 40 % or more is treated in the same way as the solid shell. The rest is modeled as a thin layer of a Newtonian fluid with large (dimensionless) viscosity $\bar{\mu}_{\mathrm{mz}}$. The shell tip $\bar{x}_s$ separates these two parts of the mushy zone. An asymptotic analysis with respect to the aspect ratio of the viscous layer yields the equation for the strand velocity $\bar{u}_{\mathrm{sh}}$:

$$\begin{aligned} \bar{x} < \bar{x}_{\mathrm{s}}: \quad & \frac{\partial}{\partial \bar{x}}\left(\bar{\mu}_{\mathrm{mz}} \frac{\partial \bar{u}_{\mathrm{sh}}}{\partial \bar{x}} \bar{d}\right) = \frac{\bar{\mu}_{\mathrm{sl}}}{2(1-\zeta_{\mathrm{s}})^2 \bar{w}}\left(\bar{u}_{\mathrm{m}}(1+2\zeta_{\mathrm{s}}) + 2\bar{u}_{\mathrm{sh}}(1-\zeta_{\mathrm{s}}) - \frac{3\bar{Q}}{\bar{w}}\right) , \\ \bar{x} \geq \bar{x}_{\mathrm{s}}: \quad & \bar{u}_{\mathrm{sh}} = \bar{U}_{\mathrm{cast}} . \end{aligned} \tag{7}$$

4 Heat transfer

Heat transfer through the mould is governed by conduction from the hot face of the mould wall to the cold face and by forced convection flow in the cooling water. Using constant material properties of the copper mould and an approximation for fully developed turbulent flow, a heat transfer coefficient between the hot face and the cooling water can easily be calculated.

Heat transfer between liquid steel and liquid slag is controlled by the fluid flow on both sides of the interface. Since the inherently three-dimensional, turbulent flow of the melt cannot be adequately described by a two-dimensional model, a non-dimensional heat transfer coefficient (Stanton number) is introduced. This Stanton number mainly depends upon the geometry of the casting mould and the entry nozzle. It can therefore be viewed as a machine-specific parameter, which is obtained either from numerical simulations of the three-dimensional melt flow in a specific casting machine or from empirical data (e.g., measurements of mould temperature or oscillation mark depth).

Convection in the slag pool is calculated within the framework of the simplified problem described in the previous section (small capillary number, constant material properties, absence of solidification) using a finite-volume code. It turns out that despite the large influence of convection and the slag pool not being slim, a reasonable approximation for the temperature profile along the interface can be obtained from horizontal conduction alone.

Heat transfer in the liquid slag gap is also approximated by horizontal conduction, neglecting the heat capacity of the slag.

The energy balance for a cross section of the strand shell is

$$\begin{aligned} \bar{d} = 0: &\qquad \bar{H}_{\mathrm{sh}} = 0\ , \\ \bar{d} > 0: &\quad \frac{\partial \bar{H}_{\mathrm{sh}}}{\partial \bar{t}} + \frac{\partial (\bar{u}_{\mathrm{sh}} \bar{H}_{\mathrm{sh}})}{\partial \bar{x}} = \frac{1}{Pe_{\mathrm{st}}} \left(\bar{h}_{\mathrm{st}} \bar{\vartheta}_{\mathrm{sup}} - \bar{q}_{\mathrm{if}} \right)\ . \end{aligned} \tag{8}$$

where $\bar{H}_{\mathrm{sh}}$ denotes the dimensionless enthalpy of a cross section of the strand shell.

5 Solidification

Slag in contact with the mould wall solidifies into a glassy or crystalline phase, depending on the cooling rate. For the sake of simplicity glassy solidification is assumed. In this case the effective thermal conductivity is similar to that of the liquid phase, and the latent heat of fusion can be neglected. This results in a linear temperature profile across the whole slag gap (solid and liquid phases). Between the solid slag and the mould wall a thermal contact resistance is introduced, representing the formation of an air gap. This air gap has been observed to account for up to 50 % of the total thermal resistance in a continuous casting mould.

Solidification of the melt is described by an enthalpy method, assuming a piecewise linear dependence of the specific enthalpy of temperature in the solid, mushy and liquid phase, respectively. An integral method is applied to solve the energy equation for the strand shell. The temperature profile in the shell is approximated by a parabola satisfying boundary conditions at the strand surface and at the liquidus isotherm. Since the energy equation does not take a particularly simple form along any border, it is not used to impose further conditions upon the assumed temperature profile.

6 Numerical implementation

Based upon the ideas presented in the previous sections, a mathematical model comprising the interaction of fluid flow, heat transfer and solidification in the meniscus region is obtained. It consists of a mixed system of algebraic, ordinary and partial differential equation for fourteen non-dimensional solution variables and sixteen non-dimensional parameters. The solution variables are functions of a vertical coordinate and time. Boundary conditions at the surface of the melt are chosen to match the static meniscus. Since only the meniscus region of a continuous casting mould is being modeled, the lower boundary is an artificial one. Boundary conditions there are chosen that influence the solution as little as possible. Initial conditions can be chosen arbitrarily as long as a stable periodic solution is obtained.

The time derivatives are discretized using implicit first and second order schemes and a constant time step. This leaves a multi-point boundary value problem of ordinary differential and algebraic equations to be solved at each time step. The solution of this problem is performed in two parts. First, a *mechanical* sub-problem of six solution variables is solved by a collocation [2] method with automatic grid refinement. Then a *thermal* sub-problem consisting of a first-order differential equation and a number of algebraic equations in the remaining eight solution variables is solved iteratively using an implicit upwind scheme on an equidistant grid and a smaller time step.

This solution algorithm is validated by solving the same physical problem with different time step sizes. Figure 4 shows the width of the flux gap evaluated after a fixed number of oscillation periods. Smaller time steps yield sharper oscillation marks and smaller numerical oscillations between the marks. For most calculations 128 time steps per oscillation period are a good choice, some sets of physical parameters however require a smaller time step.

The governing equations are integrated forward in time using a fixed time step size $\Delta\bar{t}$ and an implicit scheme for the discretization of time derivatives. Above the shell tip and in its vicinity, a first order scheme is applied for easy convergence. Sufficiently far below the shell tip, the oscillation marks are convected with the strand shell almost unchanged. This solution is particularly sensitive to numerical dissipation, therefore a second order scheme is applied in this region. In order to avoid numerical problems arising from the variation of the location of the shell tip x_s , the intervals $(\bar{x}_0, \bar{x}_\mathrm{s})$ and $(\bar{x}_\mathrm{s}, \bar{x}_\infty)$ are both mapped to the standard interval $(0, 1)$. This transformation maps the shell tip to $\xi = 0$ and both ends of the solution domain ($\bar{x} = \bar{x}_0$ and $\bar{x} = \bar{x}_\infty$) to $\xi = 1$. Additional boundary conditions at $\xi = 0$ ensure the continuity of $\bar{w}$, $\partial\bar{w}/\partial\bar{x}$, $\bar{Q}$ and $\bar{p}$. The resulting multi-point boundary value problem is solved by a collocation method [2].

6.1 Validation of the numerical scheme

In order to validate the convergence of the numerical scheme, the same physical problem has been solved with different time step sizes. The physical parameters of the test case are listed in [21].

A system of ODEs is solved in the mechanical part of each time step. The solution algorithm for this subproblem performs automatic grid refinement until certain error tolerance limits are met. The numerical parameters of the solution algorithm thus are the time step $\Delta\bar{t}$ and the error tolerance limits.

Figure 4 shows how the time step size affects one solution variable, the width of the flux gap $\bar{w}$, evaluated after a fixed number of oscillation periods. Smaller time steps yield sharper oscillation marks and smaller numerical oscillations between the marks. The average oscillation mark depth (calculated as the difference between maximum and minimum gap width in each interval between two oscillation marks) is shown in fig. 5: For large time steps, the discretization error is significant, and the average oscillation mark depth varies strongly with the time step size. For small time steps, the error allowed in the solution

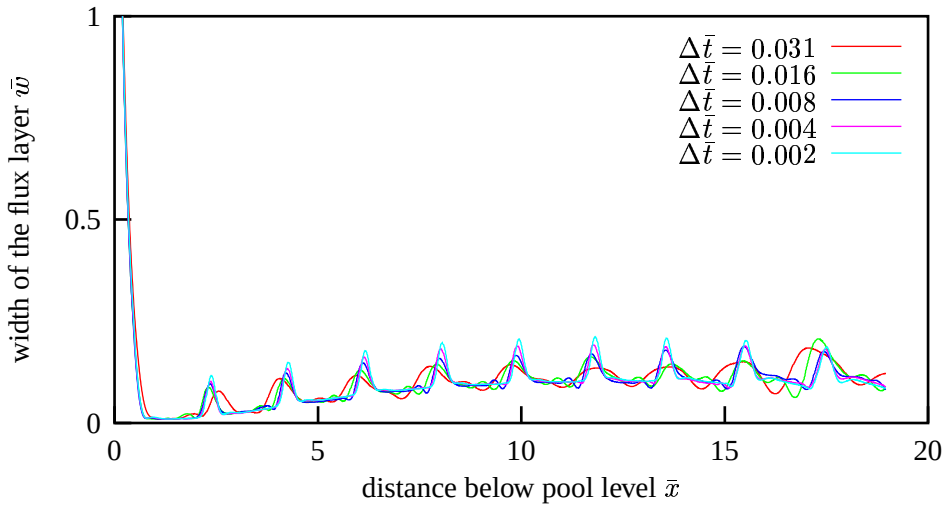

Figure 4: Influence of the time step size on the gap width

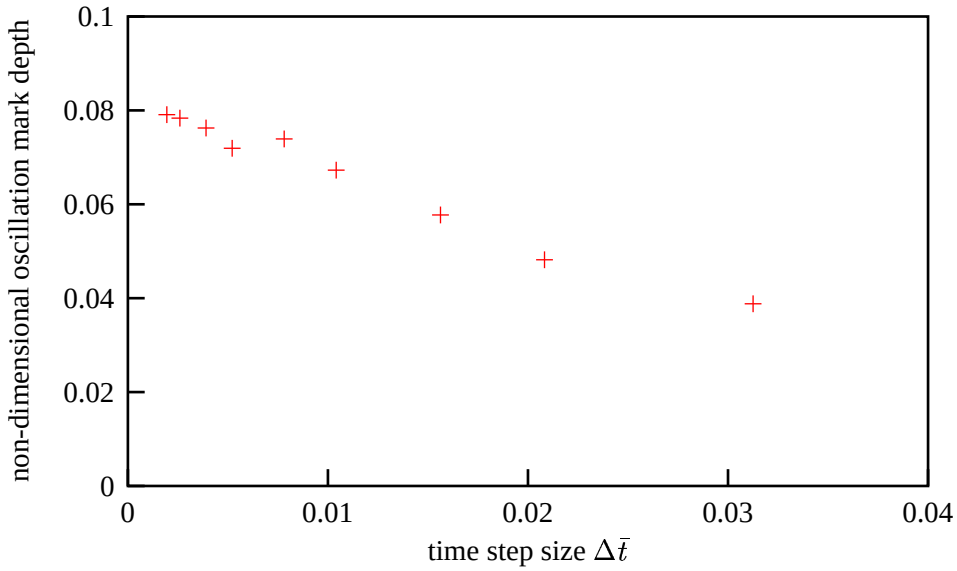

Figure 5: Influence of the time step size on the oscillation mark depth

of the ODEs exceeds the discretization error in the time derivatives. Therefore, the average oscillation mark depth remains in a narrow band, showing random variations for different time step sizes. The limit between these two regimes is around $\Delta\bar{t} = 0.01$. For the calculations presented in the following chapter, a time step size of $\Delta\bar{t} = 0.008$ (128 time steps per oscillation period) has been used. Some sets of physical parameters however required a smaller time step.

6.2 Calculating long-term averages

When performing numerical simulations of casting processes, long-term averages of quantities such as the flux powder consumption or the oscillation mark depth are of practical interest. The computational

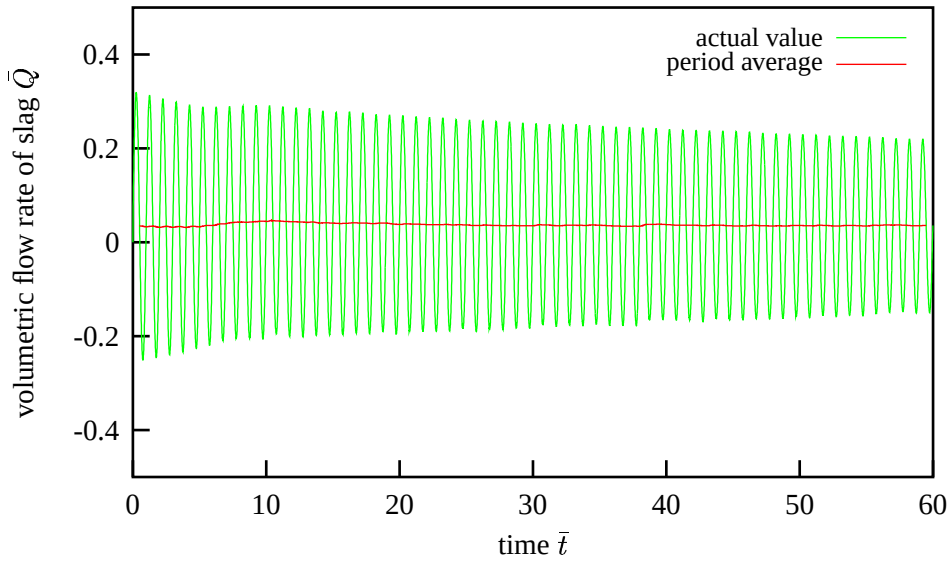

Figure 6: Regular behavior: Period-averaged volume flux remains constant.

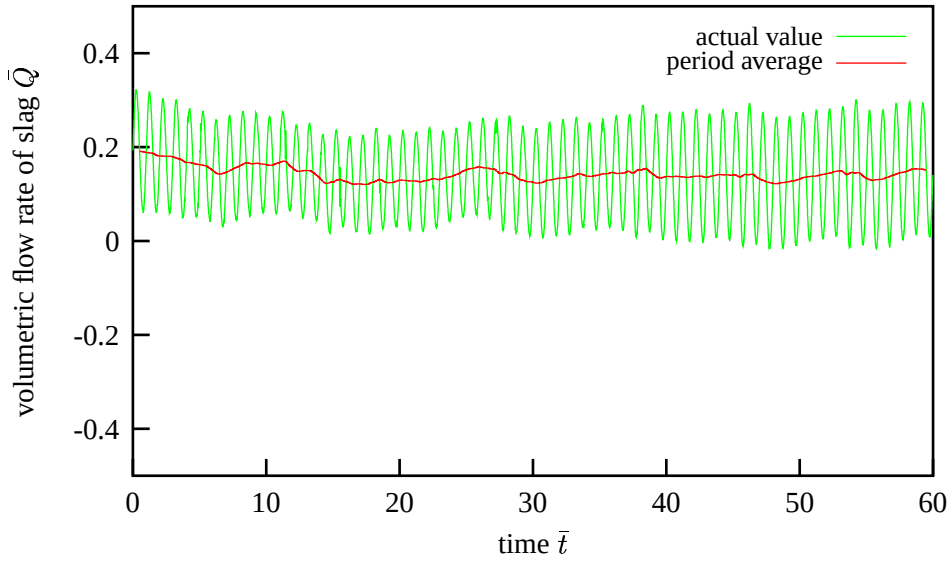

Figure 7: Irregular behavior: Period-averaged volume flux keeps changing.

effort can be reduced if a more or less periodic solution is obtained. Figure 6 shows the volumetric flow rate of slag at a fixed position below the pool level over time (green line), along with period averages (red line), for the physical parameters listed in section 6.1. Although the changes during each oscillation cycle are very large compared to the long-term average, period averages reach a fairly constant value after some 20 or 30 oscillation cycles. However, the situation is different if the oscillation frequency is reduced from 120 min^{-1} to 50 min^{-1} (fig. 7): Period averages still show substantial variations after any number of oscillation period. This irregular behavior can be observed in a number of cases. For the parametric study in section 6.1, long-term averages have been obtained by calculating period-averages for each time step and then taking the median over 20 periods.

7 Results

7.1 A representative case

This section presents numerical results for a typical set of parameter values in some detail. For complete list of parameters see [21]

Starting from an initial state a periodic solution was obtained after about 30 oscillation periods. The results shown in this section are taken from the 59^{th} oscillation period. The red line in fig. 8a shows the sinusoidal mould oscillation. Below are five snapshots of the meniscus region corresponding to the black dots along the mould oscillation line: The upper turning point, the point of maximum downward motion, the lower turning point, the point of maximum upward motion and the next upper turning point. The regions of solid and liquid slag are shaded in dark blue and light blue, respectively. The solid strand shell is marked red, the mushy zone orange, and the steel melt yellow. The regular marks in the strand surface caused by the mould oscillation can be seen very clearly. The distance between two oscillation marks is $U_{\text{cast}}/f = 10\ \text{mm}$. The average oscillation mark depth is $0.42\ \text{mm}$. The oscillation marks on the strand surface cause corresponding marks in the mushy zone, because the heat flux density and therefore the rate of solidification are substantially reduced.

The snapshots also show how these oscillation marks form: During the downstroke phase the pressure in the flux gap rises, and the thin strand shell is bent away from the mould wall. As the mould approaches the lower turning point, the ferro-static pressure of the melt prevails, beginning to bend back the shell tip: an oscillation mark forms. During the upstroke phase the flux gap closes again, the meniscus comes very close to the mould wall, and a new piece of solid shell is formed, disconnected at first from the rest of the strand shell.

It has been proposed [22] that the negative strip phase, that part of the downstroke phase in which the mould velocity exceeds the casting speed, is of particular relevance for the formation of oscillation marks and the stability of the whole casting process. The simulation results presented here suggest that in fact nothing special happens during this phase. The crucial phase rather seems to be the second half of the upstroke phase, when the flux gap becomes very thin and a new piece of solid steel is connected to the shell not by mechanical pressure in the slag but by strong cooling. This is also evident from the green line in fig. 8a, which shows the position of the shell tip: During the downstroke phase the shell tip moves downwards more or less with casting speed. During the upstroke phase the downward motion of the shell tip slows down, until the new piece of shell is connected shortly before the mould reaches the upper turning point.

Figure 9 shows time-averaged temperature profiles in the meniscus region. The strand surface temperature T_{if} is around 1400°C, the temperature of the hot face around 250°C. The thermal contact resistance at the mould wall produces a temperature drop of almost 500°C. Figure 9 also shows the heat flux density on both sides of the strand shell, q_{st} and q_{if}. The difference between the two accounts for the shell growth. Note that in our simplified model the heat flux density is constant from the cooling water to the strand surface, $q_{\text{w}} = q_{\text{m}} = q_{\text{s}} = q_{\text{l}} = q_{\text{if}}$. The heat flux density at the mould is around $2\ \text{MW}/\text{m}^2$.

A key figure for operating a continuous casting machine is the specific powder consumption m_{sl}, which is the consumption of flux powder per unit area of cast strand surface. It can be calculated from the volumetric flow rate of flux,

$$m_{\text{sl}} = \frac{\rho_{\text{sl}} Q}{U_{\text{cast}}}\ . \tag{9}$$

The time-averaged specific powder consumption for this representative case is $m_{\text{sl}} = 0.28\ \text{kg}/\text{m}^2$.

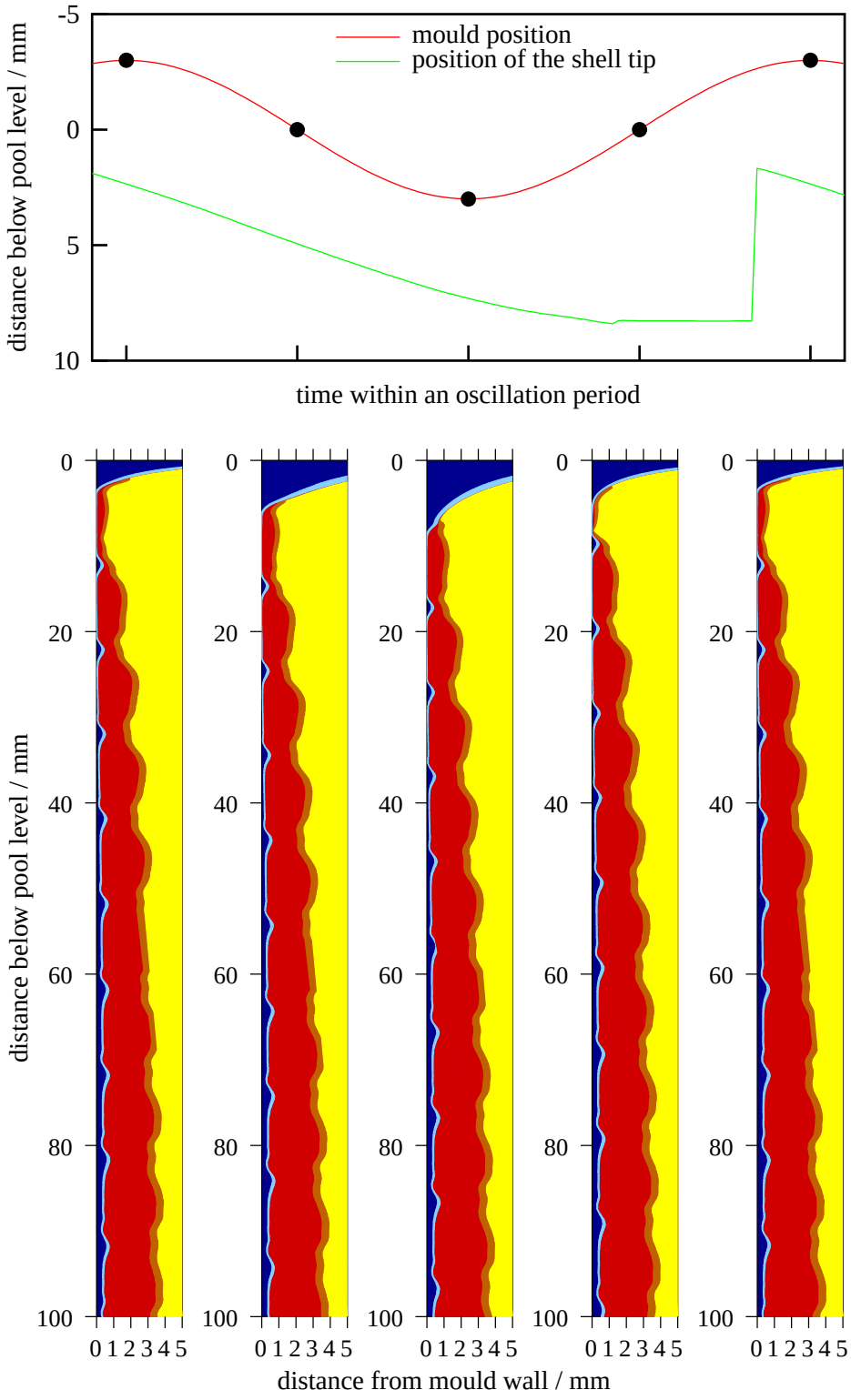

Figure 8: An oscillation cycle: *a.* sinusoidal mould oscillation and position of the shell tip, *b.* snapshots of the flux gap (blue) and the strand shell (red).

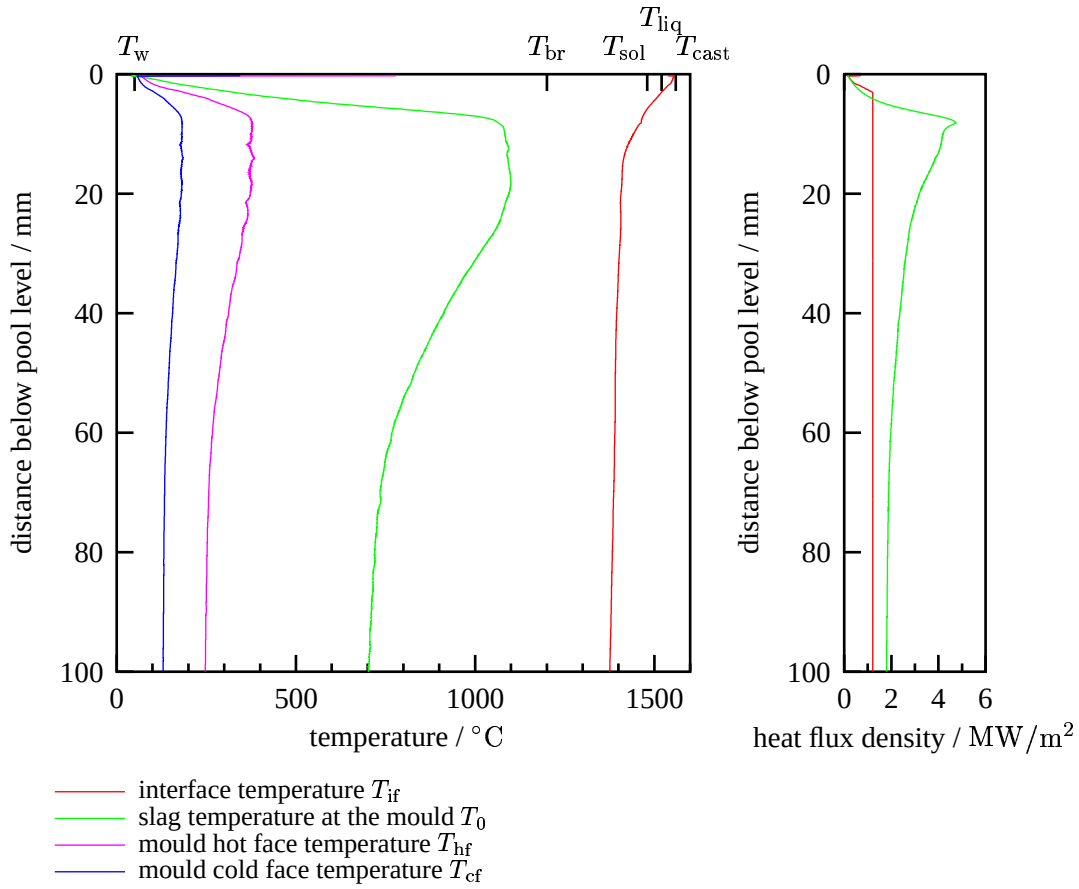

Figure 9: Time-averaged temperature and heat flux density profiles.

7.2 Parametric studies

Three oscillation parameters that are commonly used for controlling the casting process have been studied with respect to their influence on powder consumption and oscillation mark depth: the mould oscillation stroke s, the oscillation frequency f and the casting speed U_{cast}. All other parameters were kept constant.

Figure 10 shows the influence of the casting speed U_{cast} on the specific powder consumption m_{sl} for two different oscillation frequencies. The calculations show a strong decrease of the specific powder consumption with increasing casting speed. This was to be expected from (9) if the dependence of Q on U_{cast} is weaker than linear.

These calculations have also been done to test the model against experimental data [13]. The only parameter that was used for fitting is the Stanton number St_{st}, which depends strongly on the geometry of the casting machine. The results obtained for $St_{\mathrm{st}} = 0.3$ are in excellent agreement with the experimental data.

Finally, both the oscillation stroke s and the frequency f have been varied simultaneously for a fixed casting speed, $U_{\mathrm{cast}} = 1.2$ m/min. The range of values covered is 2 mm $\leq s \leq$ 9 mm and 50/min $\leq f \leq$ 200/min. Figure 11 shows that the influence of oscillation stroke and frequency on the specific powder consumption is non-monotonic. This is in agreement with the fact that contradictory trends have been reported in the literature: Most authors [23, 6, 17] report a decrease in powder consumption and/or oscillation mark depth with decreasing stroke and increasing frequency. However, in some frequency

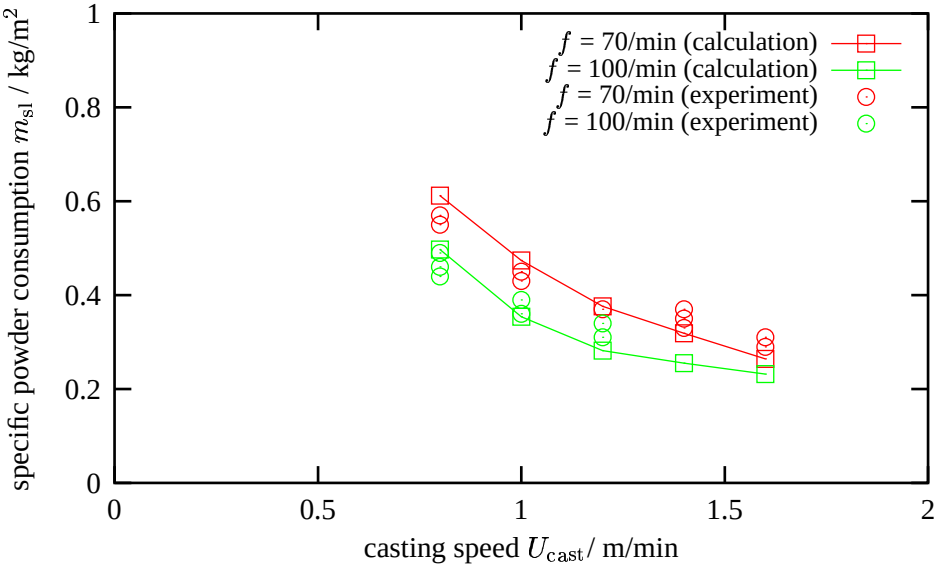

Figure 10: Calculated and measured powder consumption for various casting speeds ($s = 8$ mm).

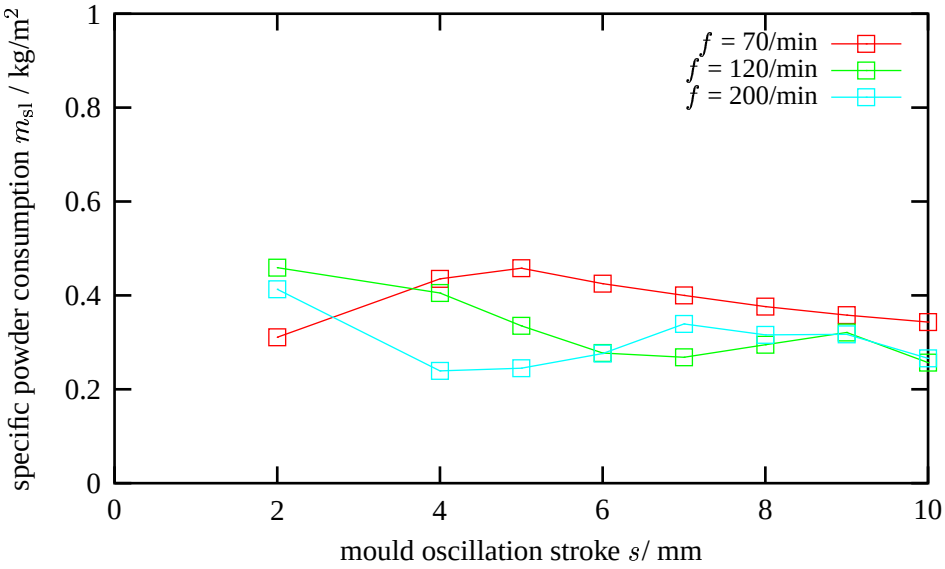

Figure 11: Calculated powder consumption for various mould oscillation strokes ($U_{cast} = 1.2$ mm).

regimes the adverse trend has also been found [11, 19].

8 Summary

A modeled based on the lubrication approximation for the slag flow has been developed to describe the entrainment of flux into the lubrication gap between the strand shell and the mould. Coupling with the heat transfer problem and a model describing the deformation of the strand shell the early stages of solidification can be described.

The model equation are very sensitive to perturbation and thus great care has to be taken by the numerical evaluation. Improvements can be made by taking temperature dependent material properties, two dimensional convective heat transfer in the meniscus region and coupling to the flow of the steel melt into account.

References

[1] E. Anzai, T. Ando, T. Shigezumi, M. Ikeda, T. Nakano, *Hydrodynamic behavior of molten powder in meniscus zone of continuous casting mold*, Nippon Steel, Technical report 34, (1987), 31-40.

[2] U. Ascher, J. Christiansen, R. D. Russell, *Collocation software for boundary-value ODEs*, ACM Trans Math Software, 7, (1981), 209-222.

[3] T. J. H. Billany, K. C. Mills, *Mould flux performance during continuous casting*, Commission of the European Communities, Directorate-General Science, Research and Development, EUR 12140 EN (1989).

[4] D. R. Bland, *Flux and the continuous casting of steel*, IMA J. Appl. Math., 32, (1984), 89-112.

[5] J. K. Brimacombe, I. V. Samarasekera, *The thermal field in continuous casting moulds*, Iron&Steelmaker Magazine, 6 (10), (1979), 20-27.

[6] A. W. Cramb, F. J. Mannion, *The measurement of meniscus marks at Bethlehem Steels Burns Harbor slab caster*, in 68^{th} *steel-making conference proceedings*, Iron and Steel Society, Warrendale, Pennsylvania, (1985), 349-359.

[7] J. A. Di Lellio, G. W. Young, *An asymptotic model of the mold region in a continuous steel caster*, Metal. Mater. Trans. B, 26B, (1995), 1225-1241.

[8] J. Dixon, A. A. Howe, I. Stewart, P. Jervis, *Reduction of reciprocation marks by high frequency vibration of the continuous casting mould*, Commission of the European Communities, EUR 10499 EN, Directorate-General Science, Research and Development, (1986).

[9] P. J. Flint, *A three-dimensional finite difference model of heat transfer, fluid flow and solidification in the continuous slab caster*, in 9^{th} *process technology,* 73^{rd} *steel-making conference proceedings*, Iron and Steel Society, Warrendale, Pennsylvania, (1990), 481-490,.

[10] I. A. Frigaard, *A mathematical model of the mould-strand gap in a steel continuous casting machine during normal operation.* Institutsbericht 490, Institut für Mathematik, Johannes-Kepler-Universität Linz, Austria (1995).

[11] S. Hiraki, K. Nakajima, T. Murakami, T. Kanazawa, *Influence of mold heat fluxes on longitudinal surface cracks during high speed continuous casting of steel slab*, in 77^{th} *steel-making conference proceedings*, Iron and Steel Society, Warrendale, Pennsylvania, (1994), 397-403.

[12] X. Huang, B. G. Thomas, F. M. Najjar, *Modeling superheat removal during continuous casting of steel slabs*, Metal. Trans. B, 23B (6), (1992), 339-356.

[13] M. Inagaki, T. Hirose, C. Matsumura, *Improvement technology of surface quality at velocity change*, CAMP-ISIJ, 2 (1989), 309.

[14] T. Inouye, K. Noro, Y. Akita, I. Katano, *Heat transfer in the continuous casting mold*, Technical Report, Nippon Steel, 12, (1978), 86-96.

[15] J. R. King, A. A. Lacey, C. P. Please, P. Wilmott, A. Zoryk, *The formation of oscillation marks on continuously cast steel*, Math. Eng. Ind., 4 (2), (1993), 91–106.

[16] J. K. Mahapatra, J. K. Brimacombe, I. V. Samarasekera, N. Walker, N., E. A. Paterson, J. D. Young, *Mold behavior and its influence on quality in the continuous casting of steel slabs: Part I. Industrial trials, mold temperature measurements, and mathematical modeling*, Metal. Trans. B. 22B (Dec) (1991), 861–874.

[17] K. Mörwald ,R. Scheidl R, C. Fürst Chr, W. Marschal *Hydraulic oscillation drive*, Report, 12^{th} Technical Exchange Meeting POSCO – VOEST-ALPINE, VOEST-Alpine Industrieanlagenbau, (1994).

[18] I. B. Risteski, *A mathematical model of the conduct of the molten powder in the gap between the mould and the slab in the vicinity of the meniscus*, Steel & Metals Mag., 28 (10), (1990), 661–665.

[19] H. Sha, *Beiträge zum Entstehungsmechanismus der Oszillationsmarken beim Stranggießen.* Ph-D thesis, Technische Universität Clausthal (1997).

[20] C. Rudischer, *The interaction between fluid flow, heat transfer and solidification in a continuous casting mould.* Ph-D thesis, University of Technology, Vienna, Austria (2001).

[21] H. Steinrück, C. Rudischer, *Mathematical Modelling of the Formation of Oscillation Marks in Continuous Casting of Steel*, to appear in J.C. Misra ed., *Topics of Industial Mathematics*, Narosa Publishing House, New Delhi, India, (2002).

[22] E. Takeuchi, J. K. Brimacombe, *The formation of oscillation marks in the continuous casting of steel slabs*, Metals Tans. B. 15B , (1984), 493–509.

[23] H. Takeuchi, S. Matsumura, R. Hidaka, Y. Nagano, Suzuki, *Effects of mould oscillation conditions on oscillation marks of stainless steel casts*, Tetsu-to-Hagane 69, (2), (1983), 248–253.

[24] B. G. Thomas, R. O'Malley R., D. Stone, *Measurement of temperature, solidification, and microstructure in a continuous cast thin slab*, Progress Report, Metal Process Simulation Laboratory, University of Illinois at Urbana-Champaign, (1998).

[25] G. Zuba, A. Preuer, H Sattler, J. Vlcek, *Complex fluid flow analysis in continuous casting*, in: *Proceedings of the* 5^{th} *international continuous casting conference*, VAI Voest-Alpine Industrieanlagenbau; Linz, Austria, (1990), 21/1-21/13.